FERMILAB-PUB-15-084-T

Vector and scalar charmonium resonances with lattice QCD

C. B. Lang,[a] **Luka Leskovec,**[b] **Daniel Mohler**[c] **and Sasa Prelovsek**[b,d,e]

[a] *Institute of Physics, University of Graz, Universitätsplatz 3, A–8010 Graz, Austria*
[b] *Jozef Stefan Institute, Jamova 39, 1000 Ljubljana, Slovenia*
[c] *Fermi National Accelerator Laboratory, P.O. Box 500, Batavia, Illinois 60510-5011, U.S.A.*
[d] *Department of Physics, University of Ljubljana, Jadranska 19, 1000 Ljubljana, Slovenia*
[e] *Theory Center, Jefferson Lab, 12000 Jefferson Avenue, Newport News, VA 23606, USA*

E-mail: christian.lang@uni-graz.at, luka.leskovec@ijs.si, dmohler@fnal.gov, sasa.prelovsek@ijs.si

Abstract: We perform an exploratory lattice QCD simulation of $D\bar{D}$ scattering, aimed at determining the masses as well as the decay widths of charmonium resonances above open charm threshold. The resulting phase shift for $D\bar{D}$ scattering in p-wave yields the well-known vector resonance $\psi(3770)$. For $m_\pi = 156$ MeV, the extracted resonance mass and the decay width agree with experiment within large statistical uncertainty. The scalar charmonium resonances present a puzzle, since only the ground state $\chi_{c0}(1P)$ is well understood, while there is no commonly accepted candidate for its first excitation. We simulate $D\bar{D}$ scattering in s-wave in order to shed light on this puzzle. The resulting phase shift supports the existence of a yet-unobserved narrow resonance with a mass slightly below 4 GeV. A scenario with this narrow resonance and a pole at $\chi_{c0}(1P)$ agrees with the energy-dependence of our phase shift. The three scenarios with just one narrow resonance, just one broad resonance, or one narrow and one broad resonance are not supported by our lattice data. Further lattice QCD simulations and experimental efforts are needed to resolve the puzzle of the excited scalar charmonia.

Keywords: decay width, charmonium, scattering, lattice QCD

Contents

1 Introduction

Charmonia $\bar{c}c$ well below open-charm threshold $\bar{D}D$ are among the best understood hadrons. Their spectra and selected transition matrix elements are successfully described by lattice QCD simulations and QCD motivated models. Recent lattice calculations have performed the necessary extrapolations and considered spectra [1, 2] as well as certain radiative transitions [3, 4]. For states well-below open charm threshold, the main remaining uncertainty is the neglect of charm-annihilation Wick contractions in lattice simulations.

The most interesting charmonium and charmonium-like states lie near or above open charm thresholds. During the past decade a plethora of states that can likely not be interpreted as conventional $\bar{c}c$ have been discovered in experiment (for a review see for example [5, 6]). These states have been treated theoretically making simplifying assumptions and reliable quantitative results for those hadrons are not available. In particular, all of the lattice simulations so far have ignored the strong decay of the charmonium resonances to a pair charmed mesons $\bar{c}c \to \bar{D}^{(*)}D^{(*)}$, which typically represents the main decay mode. Except in a few simulations [7–10], the effect of the threshold on the near-threshold states

has been neglected. The most extensive spectrum of charmonia has been obtained in simulations with $N_f = 2 + 1$ dynamical flavors at $m_\pi \simeq 400$ MeV [11], but the determination neglects the unstable nature of the states and relies on extracting the energy levels with only quark-antiquark interpolating fields, which may lead to unphysical results close to multi-hadron thresholds [12–14].

Here we present a lattice QCD simulation of the vector ($J^{PC} = 1^{--}$) and scalar (0^{++}) charmonium resonances above $\bar{D}D$ threshold, taking into account their strong decay to $\bar{D}D$ for the first time. The lowest vector resonance above open charm threshold, the $\psi(3770)$ is well established in experiment [15], and we extract its width by simulating $\bar{D}D$ scattering in p-wave. In contrast to that, the experimental and theoretical status of scalar charmonia is puzzling: the only well-established state is the ground state $\chi_{c0}(1P)$, while there is no commonly accepted candidate for its first excitation $\chi_{c0}(2P)$. We present a study of $\bar{D}D$ scattering in s-wave, aiming to address this open problem. We also consider possible effects of the $\bar{D}D$ threshold on the vector $\psi(2S)$ and scalar χ_{c0} charmonia, which lie below threshold.

2 Open questions for charmonia of interest

2.1 Vector charmonia

The $\psi(3770)$ with $M = 3773.15 \pm 0.33$ MeV and $\Gamma = 27.2 \pm 1.0$ MeV is located only $\simeq 45$ MeV above $\bar{D}D$ threshold [15, 16]. We focus here on its dominant decay mode $\psi(3770) \to \bar{D}D$ in p-wave with branching fraction 0.93^{+8}_{-9} [15]. It is a well-established experimental resonance and is generally accepted to be predominantly the conventional ${}^{2s+1}nL_J = {}^3 1D_1$ $\bar{c}c$ state [17–19]. There is an ongoing discrepancy between results from BES-II [20] and Cleo [21] regarding the non-$\bar{D}D$ part of the branching fraction which may be connected to neglecting interference effects in the BES-II analysis. Significant non-$\bar{D}D$ decays into light hadrons can occur if there is non-negligible mixing with the $\psi(2S)$ [22]. For our analysis we neglect disconnected contributions that would cause decay into light hadrons and treat the decay into $\bar{D}D$ as elastic, neglecting the decays into $J/\psi\,\pi\pi$ and $J/\psi\,\eta$ that have tiny branching fractions [15]. Our aim is to perform the first determination of the $\psi(3770)$ resonance mass and $\psi(3770) \to \bar{D}D$ decay width using a lattice simulation for $\bar{D}D$ scattering in p-wave.

We also investigate whether the $\bar{D}D$ threshold has any effect on $\psi(2S)$, which is the first radial excitation of J/ψ and is situated $\simeq 42$ MeV below threshold. Such a possibility was discussed in relation to the Fermilab-MILC preliminary results [23] where a simple analysis of the spin-averaged $2S$ state appeared high with respect to experiment, although large systematic uncertainties related to excited state contaminations were observed. A more recent HPQCD study [2] finds no significant discrepancy. The mixing of the vector charmonia with a pair of two charmed mesons was first simulated in [7], where only $D_1\bar{D}$ in s-wave was considered and the width of $\psi(3770)$ was not extracted.

2.2 Scalar charmonia

The only well established scalar charmonium state is the ground state $\chi_{c0}(1P)$, interpreted as the $^3 1P_0$ $\bar{c}c$ and located well below the open charm threshold. A further known resonance, the $X(3915)$ with $\Gamma = 20 \pm 5$ MeV is seen only in $J/\psi\,\omega$ and $\gamma\gamma$ decay channels [15]. BaBar has determined its J^P quantum numbers to be 0^+ [24] which would only allow $J^{PC} = 0^{++}$. This spin-parity determination by BaBar assumes that a $J^P = 2^+$ resonance would be produced in the helicity 2 state, which might not be justified for an exotic meson [5]. As a consequence, the PDG recently assigned $X(3915)$ to be $\chi_{c0}(2P)$ [15], but a number of convincing reasons given by Guo & Meissner [25] and Olsen [26] raise serious doubts about this assignment:

- The dominant decay mode of scalar charmonium above open charm threshold is expected to be a "fall-apart" mode into $\bar{D}D$ that would lead to a relatively broad resonance. In particular the width into $\bar{D}D$ is expected to be much larger than for the well-established $\chi_{c2}(2P)$ [15], which decays to $\bar{D}D$ in d-wave. Yet $m_{D\bar{D}}$ invariant mass spectra of several experiments show no evidence for $X(3915) \to D\bar{D}$. This also indicates that the $\bar{D}D$ width extracted from the present lattice simulation cannot be compared to $X(3915)$.

- The spin-splitting $m_{\chi_{c2}(2P)} - m_{\chi_{c0}(2P)}$ within this assignment seems too small compared to $m_{\chi_{b2}(2P)} - m_{\chi_{b0}(2P)}$ or $m_{\chi_{c2}(1P)} - m_{\chi_{c0}(1P)}$.

- The partial width for the OZI suppressed $X(3915) \to \omega J/\psi$ seems too large [25], which is translated to two contradicting limits for this decay in [26].

The intriguing $\chi_{c0}(2P)$ was related to the broad structures in $\bar{D}D$ invariant mass in the same references [25, 26]. The process $\gamma\gamma \to \bar{D}D$ from BaBar [27] and Belle [28] leads Guo&Meissner to[1]

$$[25]: \quad m = 3837.6 \pm 11.5 \text{ MeV}, \ \Gamma = 221 \pm 19 \text{ MeV}, \tag{2.1}$$

while $e^+e^- \to J/\psi\, D\bar{D}$ from Belle [29] leads Olsen to

$$[26]: \quad m = 3878 \pm 48 \text{ MeV} \ , \ \Gamma = 347 \, ^{+316}_{-143} \text{ MeV}. \tag{2.2}$$

Obviously the spectrum of scalar charmonia beyond the ground state presents an open question. Our aim is to shed light on this issue by simulating $\bar{D}D$ scattering in s-wave on the lattice, and look for possible resonances in the extracted scattering matrix. Preliminary results based on the same simulation and only one ensemble have been presented in Ref. [30].

3 Lattice setup and charm-quark treatment

The simulation is performed on two lattice ensembles with the parameters listed in Table 1. Both ensembles have rather low $m_\pi L$ but this is not a serious issue for charmonia and

[1] Here possible feed-down from $\gamma\gamma \to D^*\bar{D}$ followed by $D^* \to D\pi(\gamma)$ is ignored according to [29].

	Ensemble (1)	Ensemble (2)
$N_L^3 \times N_T$	$16^3 \times 32$	$32^3 \times 64$
N_f	2	2+1
a [fm]	0.1239(13)	0.0907(13)
L [fm]	1.98(2)	2.90(4)
m_π [MeV]	266(3)(3)	156(7)(2)
Lm_π	2.68(3)	2.29(10)
κ_c (val)	0.12300	0.12686
#configs	279	196

Table 1. The gauge configurations of ensemble (1) are from [31, 32]. Those of ensemble (2) are provided by the PACS-CS collaboration [33]. N_L and N_T denote the number of lattice points in spatial and time directions, N_f the number of dynamical flavors and a the lattice spacing.

$\bar{D}D$ scattering in this simulation, where pions do not enter explicitly. Further details about the ensembles and our implementation of charm quarks may be found in [12, 14, 31, 32] for ensemble (1) and in [33, 34] for ensemble (2).

To minimize heavy-quark discretization effects at finite lattice spacing the Fermilab method [35, 36] is used for the charm quarks. The corresponding dispersion relation [37] for a meson M containing charm quarks is

$$E_M(p) = M_1 + \frac{\mathbf{p}^2}{2M_2} - \frac{a^3 W_4}{6}\sum_i p_i^4 - \frac{(\mathbf{p}^2)^2}{8M_4^3} + \dots \ , \tag{3.1}$$

where $\mathbf{p} = \frac{2\pi}{L}\mathbf{q}$ and $\mathbf{q} \in N^3$.

On both ensembles the charm quark hopping parameter κ_c is tuned [14, 34] using the spin-averaged charmonium mass

$$\bar{m} \equiv \frac{1}{4}(m_{\eta_c} + 3m_{J/\psi}) \ , \quad \bar{m}^{exp} = 3.06859(17) \text{ GeV} \tag{3.2}$$

which is the relevant reference mass for our spectra of charmonium. The $M_{1,2,4}$ for the spin-averaged charmonium were determined based on the lattice data from the lattice dispersion relation (3.1), setting W_4 to zero. Then κ_c was fixed by tuning the kinetic mass M_2 to $\bar{m}^{exp}$. The corresponding values for the spin-averaged M_1 are given in Table 2.

To investigate the $\bar{D}D$ scattering we need the dispersion relation $E_D(p)$ for D mesons, which is also given by Eq. (3.1) with parameters $M_{1,2,4}$ in Table 2. The common feature of spectra in the scalar and vector charmonium channel are two-particle states $\bar{D}D$ that have a discrete spectrum on the finite lattice. In the absence of interactions, $D(q)\bar{D}(-q)$ have energies according to (3.1)

$$E^{n.i.}_{D(q)\bar{D}(-q)} = 2E_D(\mathbf{q}\tfrac{2\pi}{L}) \ , \quad \mathbf{q} \in N^3 \ , \tag{3.3}$$

which will be shifted due to the interaction.

Within the Fermilab approach, the rest masses have large discretization effects but mass differences are expected to be close to physical [38, 38] and can be compared to

meson	mass	Ensemble (1)	Ensemble (2)
D	$aM_1 \equiv am_D$	0.9792(11)	0.75317(83)
D	aM_2	1.107(14)	0.840(22)
D	aM_4	1.060(44)	0.95(15)
spin-aver. $\bar{c}c$	$aM_1 \equiv a\bar{m}$	1.52451(44)	1.20444(15)
$\bar{D}D$ vs. $\bar{c}c$	$2m_D - \bar{m}$	0.6910(36)	0.6568(36)

Table 2. The parameters in the dispersion relation (3.1) for D mesons and spin-averaged charmonium $\frac{1}{4}(m_{\eta_c} + 3m_{J/\psi})$. The last line is in GeV, others in lattice units.

experiment. In order to compare the splitting $E^{lat} - \bar{m}^{lat}$ with $E^{exp} - \bar{m}^{exp}$, we will sometimes plot

$$E = E^{lat} - \bar{m}^{lat} + \bar{m}^{exp} \tag{3.4}$$

and compare it with E^{exp}.

An important quantity is the position of the $\bar{D}D$ threshold with respect to our reference mass. The splitting $2m_D - \bar{m}$ for ensemble (2) is very close to the experimental value $2m_D^{exp} - \bar{m}^{exp} \simeq 0.666$ GeV, while it is a bit larger for ensemble (1) due to the heavier pion mass and larger discretization effects (see Table 2).

Our charm quark treatment has been verified on ensemble (1) for low-lying charmonia, D meson resonances [14] and D_s mesons [34, 39], where reasonable agreement with experiment was found. The spectrum for D_s mesons and some other hadrons containing charm quarks were also determined on ensemble (2) [34, 39] with even better agreement due to the lower pion mass and smaller discretization effects.

4 Analysis details

Interpolating fields O are used to create and annihilate the physical system with $J^{PC} = 1^{--}$ or 0^{++}, isospin $I = 0$ and total momentum zero. All quark fields in the interpolators are smeared according to the distillation method $q \equiv \sum_{k=1}^{N_v} v^{(k)} v^{(k)\dagger} q_{point}$ [40, 41]. We use $N_v = 192$ eigenvectors of the lattice laplacian $v^{(k)}$ for ensemble (2) and $N_v = 96$ or 64 for ensemble (1). The distillation method is convenient for calculating a variety of Wick contractions. The full distillation method [40] is employed on ensemble (1) with a smaller volume and details of the implementation are given in [12, 14]. The stochastic version [41] is used on ensemble (2) with larger volume and details of our implementation are provided in [34].

4.1 Vector channel

$\bar{D}D$ in p-wave is the dominant two-meson contribution for $E \leq 4$ GeV, while $D_1\bar{D}$ appears higher. Sixteen $\bar{c}c$ and two $\bar{D}D$ interpolating fields are used in the relevant irreducible

representation T_1^{--}:

$$\begin{aligned}
O_{1-14}^{\bar{c}c} &= \bar{c}A_i c\,, \\
O_{15}^{\bar{c}c} &= R_{ijk}\bar{c}\gamma^j E^k c\,, \quad E_i \equiv Q_{ijk}\overleftrightarrow{\nabla}_j\overrightarrow{\nabla}_k\,, \\
O_{16}^{\bar{c}c} &= R_{ijk}\bar{c}\gamma_t\gamma^j E^k c\,, \\
O_1^{DD} &= [\bar{c}\gamma_5 u(e_i)\ \bar{u}\gamma_5 c(-e_i) \\
&\quad - \bar{c}\gamma_5 u(-e_i)\ \bar{u}\gamma_5 c(e_i)] + \{u\to d\}\,, \\
O_2^{DD} &= [\bar{c}\gamma_5\gamma_t u(e_i)\ \bar{u}\gamma_5\gamma_t c(-e_i) \\
&\quad - \bar{c}\gamma_5\gamma_t u(-e_i)\ \bar{u}\gamma_5\gamma_t c(e_i)] + \{u\to d\}\,,
\end{aligned} \tag{4.1}$$

where i denotes polarization, while Q_{ijk} and $R_{ijk} = R_{jik}$ are listed in [42]. The $\bar{c}c$ interpolators $O_{1-14}^{\bar{c}c}$ for vector channel T_1^{--} are listed in Table X of [14]. The momentum is projected for each D meson separately,

$$\bar{u}\Gamma c(\mathbf{k}) \equiv \sum_{\mathbf{x}} e^{i2\pi\mathbf{k}\cdot\mathbf{x}/L}\bar{u}(\mathbf{x},t)\Gamma c(\mathbf{x},t)\,, \tag{4.2}$$

so that the O^{DD} couple to p-wave. For ensemble (1) $N_v = 64$ is used for O_2^{DD}, and $N_v = 96$ for the remaining interpolators.

The irreducible representation T_1^{--} contains $J^{PC} = 1^{--}$ states of interest, and also ψ_3 states with $J^{PC} = 3^{--}$ coupling due to the broken rotational symmetry on the lattice. In the continuum limit, $O_{1-14}^{\bar{c}c}$ contain only 1^{--}, while $O_{15,16}^{\bar{c}c}$ contain 1^{--} and 3^{--} [42], which will help us to identify the spin 3 admixture related to ψ_3.

4.2 Scalar channel

$\bar{D}D$ in s-wave and $J/\psi\,\omega$ are the dominant two-meson states in the energy region of interest $E \le 4$ GeV. Seven $\bar{c}c$, four $\bar{D}D$, and two $J/\psi\,\omega$ interpolating fields are used in the relevant irreducible representation A_1^{++}:

$$\begin{aligned}
O_{1-7}^{cc} &= \bar{c}Ac\,, \\
O_1^{DD} &= \bar{c}\gamma_5 u(0)\ \bar{u}\gamma_5 c(0) + \ \{u\to d\}\,, \\
O_2^{DD} &= \bar{c}\gamma_5\gamma_t u(0)\ \bar{u}\gamma_5\gamma_t c(0) + \ \{u\to d\}\,, \\
O_3^{DD} &= \sum_{e_k=\pm e_{x,y,z}} \bar{c}\gamma_5 u(e_k)\ \bar{u}\gamma_5 c(-e_k) + \ \{u\to d\}\,, \\
O_4^{DD} &= \sum_{|u_k|^2=2} \bar{c}\gamma_5 u(u_k)\ \bar{u}\gamma_5 c(-u_k) + \ \{u\to d\}\,, \\
O_1^{J/\psi\,\omega} &= \sum_j \bar{c}\gamma_j c(0)\ [\bar{u}\gamma_j u(0) + \ \{u\to d\}]\,, \\
O_2^{J/\psi\,\omega} &= \sum_j \bar{c}\gamma_j\gamma_t c(0)\ [\bar{u}\gamma_j\gamma_t u(0) + \ \{u\to d\}]\,.
\end{aligned} \tag{4.3}$$

$O_{1-7}^{\bar{c}c}$ are listed in Table X of [14]. The momenta are projected for each meson separately in O^{DD} and $O^{J/\psi\,\omega}$. For ensemble (1) $N_v = 64$ is used for $O_{2,3}^{DD}$, $O_2^{J/\psi\,\omega}$, and $N_v = 96$ for the remaining interpolators.

The irreducible representation A_1^{++} contains $J^{PC} = 0^{++}$ states of interest, and in general also states with $J \geq 4$, which appear at energies beyond our interest.

The interpolator O_4^{DD} is not used for ensemble (1) since $D(2)D(-2)$ appears above 4 GeV. The $O^{J/\psi\,\omega}$ are not used on ensemble (2) since the results from ensemble (1) indicate that $J/\psi\,\omega$ is almost decoupled from the rest of the system.[2]

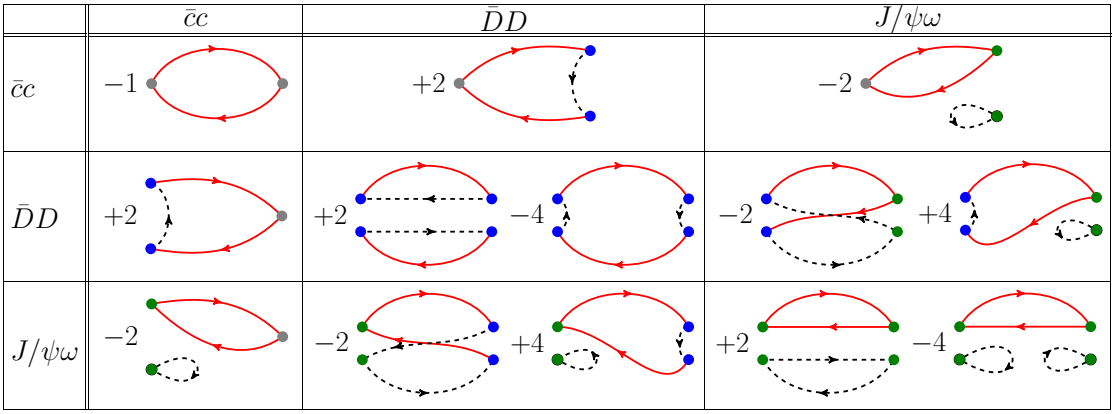

Figure 1. Wick contractions computed for the correlation matrix (4.4) with interpolators (4.1,4.3). We omit contractions where the charm quark annihilates. A red solid line represents a c quark, while the black dashed line represents a u or d quark.

4.3 Towards the spectrum

The correlation matrix

$$\begin{aligned} C_{jk}(t) &= \langle \Omega | O_j(t'+t) O_k^\dagger(t') | \Omega \rangle \\ &= \sum_n Z_j^n Z_k^{n*}\ e^{-E_n t} \end{aligned} \tag{4.4}$$

contains the information on energies E_n and the overlaps $Z_j^n \equiv \langle \Omega | \mathcal{O}_j | n \rangle$. We evaluate all Wick contractions for $O \simeq \bar{c}c$, $(\bar{q}c)(\bar{c}q)$, $(\bar{c}c)(\bar{q}q)$ (4.1,4.3) shown in Fig. 1. We omit Wick contractions where charm quark annihilates as in almost all previous lattice simulation of charmonia; these induce mixing with $I = 0$ decay channels containing only light quarks u, d, s, they are Okubo-Zweig-Iizuka suppressed and present a challenge for current lattice simulations. It is noteworthy that these decays might be important to clarify the experiment puzzle with regard to non-$\bar{D}D$ hadronic decays [18, 22].

The energies and overlaps are extracted from the correlation matrix using the generalized eigenvalue method [43–46]

$$C(t) u^{(n)}(t) = \lambda^{(n)}(t) C(t_0) u^{(n)}(t)\ , \tag{4.5}$$

[2] When the interpolators $O^{J/\psi\,\omega}$ are removed from the interpolator basis, the energies E_n and overlaps $\langle O_k | n \rangle$ for the remaining eigenstates n are practically unchanged for ensemble (1).

where $\lambda^{(n)}(t) \propto e^{-E_n t}$ at large t. Correlated two or one-exponential fits to $\lambda^{(n)}(t)$ are used and $t_0 = 2,\ 3$. The errors-bars correspond to statistical errors obtained using single-elimination jack-knife.

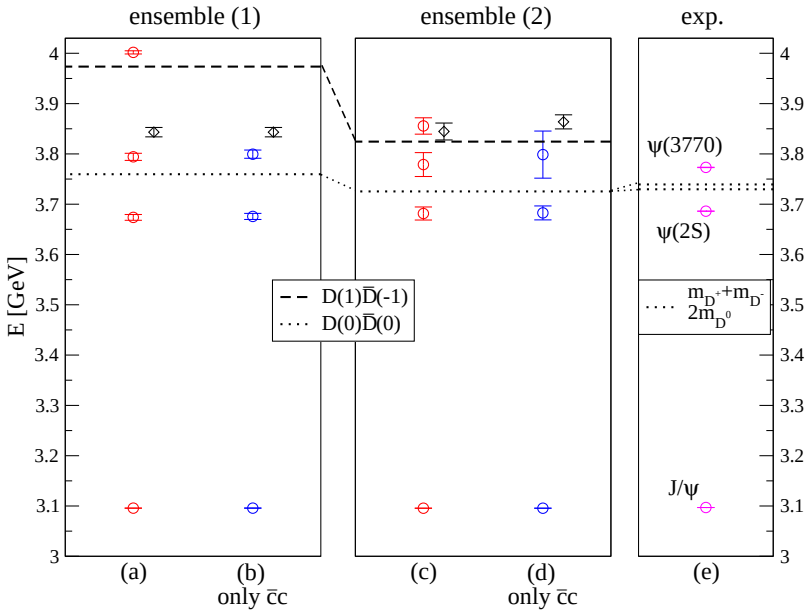

Figure 2. The energies E (see Eq. (3.4)) in the vector channel on both ensembles, together with the experimental masses. The circles represent $J^{PC} = 1^{--}$ states, while the diamond represents a 3^{--} admixture present in the irreducible representation T_1^{--} and related to the ψ_3. The dashed lines show the non-interacting energy of $D(1)\bar{D}(-1)$ (3.3), and the dotted line represents the threshold $2m_D$. The $D(0)\bar{D}(0)$ state does not appear for p-wave. Interpolators used in (a,c) are given in Table 3, while (b,d) utilize just $O^{\bar{c}c}$ from the same sets.

5 Results for the vector channel

5.1 Discrete spectrum

The energy levels in the vector channel are shown in Fig. 2a and 2c together with the experimental masses. The full set of operators gave noisier signals than suitable subsets, and the chosen subsets are listed in Table 3. The circles denote the energy levels that are related to $J^{PC} = 1^{--}$ states J/ψ, $\psi(2S)$, $\psi(3770)$, $D(1)D(-1)$ (from bottom to top), while $D(0)\bar{D}(0)$ does not appear for p-wave. The diamond indicates a level related to the $J^{PC} = 3^{--}$ state ψ_3, that is present in representation T_1^{--} due to the broken rotational symmetry on the lattice.

The highest state ($n = 5$) has largest overlap with O^{DD} and disappears when these interpolators are excluded from the basis, as shown in Fig. 2b and 2d. Each energy level in addition to $D(1)\bar{D}(-1)$ indicates the presence of a bound state or a resonance. Good resemblance with the experimental spectrum is indeed confirmed in Fig. 2. The J/ψ is significantly below threshold and no effect from threshold is expected. The $\psi(2S)$ is situated

n	fit range	fit type	$\frac{\chi^2}{d.o.f.}$	$E^{lat}a$	E [GeV] (3.4)	$(ap)^2$	$(ap)^3\cot(\delta)$	$\frac{(ap)^3\cot(\delta)}{\sqrt{s}}$	$\delta[^\circ]$
	Ens.	(1)							
1	3-14	$2e^c$	8.57/8	1.54153(43)	3.09572(34)	/	/	/	/
2	3-14	$2e^c$	16.62/8	1.9045(38)	3.6738(58)	−0.0588(47)	0.0137(18)	0.00717(95)	−109.1(6.4)i
3	3-13	$2e^c$	5.18/7	1.9801(46)	3.7941(71)	0.02413(57)	−0.00599(34)	−0.00303(17)	148.0(7.7)
4	3-13	$2e^c$	5.09/7	2.0109(60)	3.8433(93)	/	/	/	/
5	3-13	$2e^c$	8.49/7	2.1105(21)	4.0019(32)	0.1755(33)	−0.144(23)	−0.068(11)	153.0(4.4)
	Ens.	(2)							
1	3-29	$2e^c$	3.15/23	1.21683(16)	3.09557(18)	/	/	/	/
2	3-11	$2e^c$	3.44/5	1.4862(60)	3.682(13)	−0.0169(50)	0.0021(10)	0.00143(68)	120(25)i
3	3-11	$2e^c$	4.36/5	1.531(11)	3.779(24)	0.0207(93)	0.00056(255)	0.00037(167)	79(40)
4	3-11	$2e^c$	4.92/5	1.5611(78)	3.845(17)	/	/	/	/
5	3-11	$2e^c$	4.78/5	1.5661(75)	3.856(16)	0.0509(65)	−0.0054(76)	−0.0034(49)	115(35)

Table 3. Discrete lattice spectrum from charmonium in the irreducible representation T_1^{--} which contains $J^{PC} = 1^{--}$, 3^{--} and higher J states. The p and δ correspond to $\bar{D}D$ scattering in p-wave. Subset $O^{\bar{c}c}_{1-6,8,9,11,12,15}, O^{DD}_{17,18}$ from the interpolators in Eq. (4.1) is used for ensemble (1) and $O^{\bar{c}c}_{1,3-5,9-11,13,15}, O^{DD}_{17}$ for ensemble (2). $t_0 = 2$ is used for all data points.

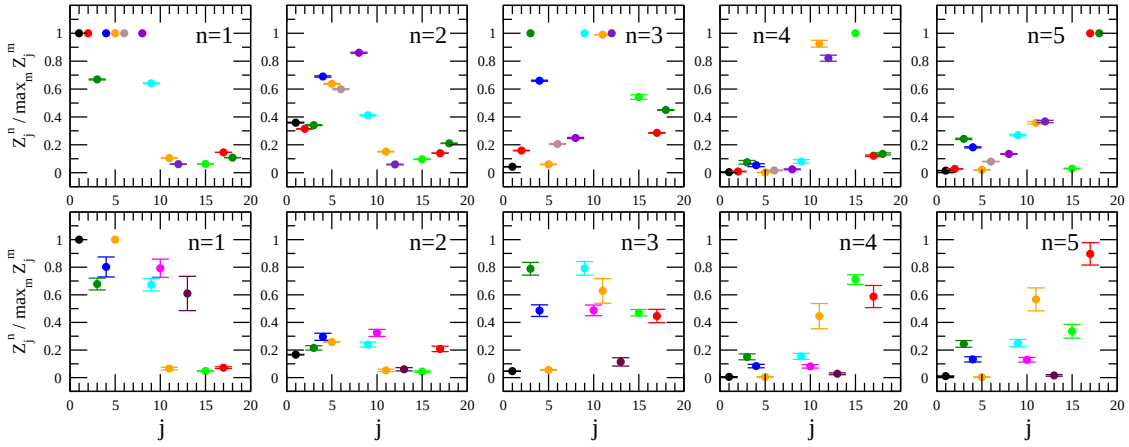

Figure 3. The overlaps $Z_j^n = \langle\Omega|\mathcal{O}_j|n\rangle$ for the vector channel show the matrix elements of interpolators $\mathcal{O}_j$ between the vacuum $\langle\Omega|$ and the physical eigenstate $|n\rangle$ on the lattice. We present the overlap ratios $Z_j^n/\max_m Z_j^m$ on ensemble (1) (top) and on ensemble (2) (bottom). The denominator is the maximal $|Z_j^m|$ at given operator number j. These ratios are independent on the normalization of the interpolators O_j. Levels $n = 1, .., 5$ are ordered from lowest to highest E_n in Figs. 2a and 2c for both ensembles, respectively. The order of interpolators j on the abscissa (listed in caption of Fig. 3) is the same as in the list (4.1).

$\simeq$ 42 MeV below threshold in experiment, and the corresponding finite volume energy on the lattice does not depend (within uncertainties) on whether $\bar{D}D$ interpolators are used or not (see Fig. 2). The appearance of levels $n = 3$ and 4 is related to the $\psi(3770)$ resonance and to the spin 3 admixture and the corresponding ψ_3 resonance. Level $n = 4$ is related to ψ_3 due to smaller overlaps $\langle O^{\bar{c}c}_{1-14}|n = 4\rangle$. This is based on the fact that $O^{\bar{c}c}_{1-14}$ couple

ground st.	Ensemble (1)	Ensemble (2)
$E^{lat}a$	2.0124(38)	1.559(51)

Table 4. The energy of ψ_3 with $J^{PC} = 3^{--}$ from the ground state in the A_2^{--} irreducible representation of the O_h point group.

in the continuum limit only to 1^{--} (which is responsible for small $\langle O^{\bar{c}c}_{1-14}|\psi_3\rangle$ at finite a), while $O^{\bar{c}c}_{15,16}$ couple to 1^{--} and 3^{--}. Further support is given by the near-degeneracy with the energies from the irreducible representation A_2^{--} where a 3^{--} state comes as the ground state (see Table 4). For the $\psi(3770)$ the avoided-level crossing scenario suggests E_3 in the energy region $m \pm \Gamma$, which is reasonably satisfied by comparing to experiment. In order to really determine the resonance mass and width for $\psi(3770)$ one needs to consider the phase shifts for $\bar{D}D$ scattering in p-wave.

5.2 $\bar{D}D$ scattering in p-wave

We assume that $\bar{D}D$ scattering in p-wave near the resonance $\psi(3770)$ is elastic, which is a good approximation since $Br[\psi(3770) \to D\bar{D}] = 93 \pm 9\%$, while the remaining part goes mainly to $J/\psi\pi\pi$. In the elastic case, the scattering phase shift δ is given by Lüscher's relation [47, 48]

$$p \cot \delta(p) = \frac{2Z_{00}(1; (\frac{pL}{2\pi})^2)}{L\sqrt{\pi}} \ , \tag{5.1}$$

which applies for the total momentum zero employed in our case. The momentum p of D mesons is extracted from the measured energy levels $E_n^{lat} = 2E_D(p)$ using the dispersion relation (3.1). The resulting momenta and phase shifts for all eigenstates except for the spin 3 admixture and for the finite volume state related to J/ψ are collected in Table 3. The large absolute value of $p^3 \cot \delta$ corresponds to feeble scattering, while small $p^3 \cot \delta$ is related to significant scattering.

We fit our data in two ways:

(i) A resonance $\psi(3770)$: The scattering matrix in the vicinity of a resonance has a Breit-Wigner form

$$T_l(s) = \frac{\sqrt{s}\,\Gamma(s)}{m_R^2 - s - i\sqrt{s}\,\Gamma(s)} = \frac{1}{\cot \delta_l(s) - i} \ . \tag{5.2}$$

The width

$$\Gamma(s) = \frac{g^2}{6\pi}\frac{p^3}{s} \tag{5.3}$$

is parametrized in terms of the phase space for p-wave decay and the $\psi(3770) \to D\bar{D}$ coupling g. It is expected that g depends only mildly on $m_{u/d}$, and that the leading dependence of Γ on $m_{u/d}$ is captured by phase space. Equations (5.2, 5.3) lead to $p^3 \cot \delta_1(s)/\sqrt{s} = (6\pi/g^2)(m_R^2 - s)$ and then expressing $s = 2(m_D^2 + p^2)^{1/2}$ and $m_R = 2(m_D^2 + p_R^2)^{1/2}$ to

$$\frac{p^3 \cot \delta(s)}{\sqrt{s}} = \frac{6\pi}{g^2} 4(p_R^2 - p^2) \tag{5.4}$$

	Ensemble (1)		Ensemble (2)		exp
	fit (i)	fit (ii)	fit (i)	fit (ii)	$D^+D^-/D^0\bar{D}^0$
$\psi(3770)$					
p_R [GeV]	0.208(31)(3)	0.159(35)(2)	0.334(155)(5)	0.343(184)(5)	0.26/0.29
m_R [GeV]	3.784(7)(10)	3.774(6)(10)	3.786(56)(10)	3.789(68)(10)	3.77315(33)
g (no unit)	13.2(1.2)	19.7(1.4)	24(19)	28(21)	18.7(1.4)
$\psi(2S)$					
$\|p_B\|$ [GeV]		0.380(17)(6)		0.280(43)(4)	0.31/0.28
m_B [GeV]		3.676(6)(9)		3.682(13)(9)	3.686109^{+12}_{-14}

Table 5. Parameters of the resonance $\psi(3770)$ and bound state $\psi(2S)$ from fits (i) (5.4) and (ii) (5.6). The $\psi(3770) \to D\bar{D}$ width $\Gamma = g^2p^3/(6\pi s)$ is parametrized in terms of the coupling g and compared the value of the coupling derived from experiment [15]. The p_R denotes D-meson momenta at the peak of the resonance and $|p_B|$ the binding momentum. The first errors are statistical and the second errors (where present) are from the scale setting uncertainty. The experimental data and errors are based on PDG values. Errors on experimental $p_{R/B}$ are suppressed as they are very small.

where p_R is the D meson momentum at the resonance peak. The values of g and p_R follow from the linear fit (5.4) through the energy levels $n = 3, 5$ in the vicinity of the resonance, where the Breit-Wigner form applies (level 4 is omitted since it is attributed to ψ_3 as discussed above). The fit is shown in Fig. 4, while the resulting resonance parameters are given in Table 5. The resonance mass m_R corresponding to the p_R on the lattice is given by inserting the Fermilab dispersion relation (3.1) in (3.4)

$$m_{R/B} = 2E_D(p_{R/B}) - \bar{m}^{lat} + \bar{m}^{exp} \tag{5.5}$$

and will be used for resonances or bound states throughout this work.

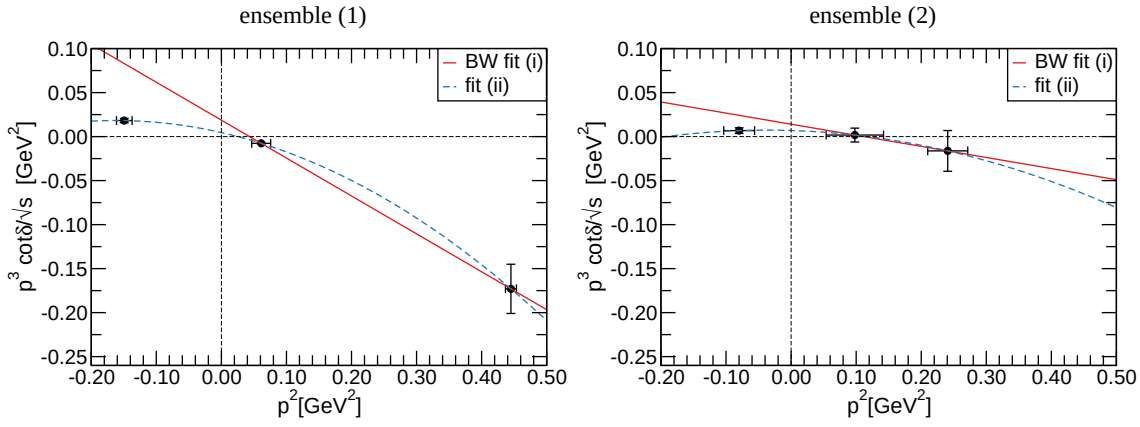

Figure 4. $p^3 \cot\delta/\sqrt{s}$ versus p^2 for $\bar{D}D$ scattering in p-wave in the region of the $\psi(2S)$ bound state and the $\psi(3770)$ resonance. The p denotes the momentum of D meson. We show the Breit-Wigner fit (i) and the extended fit (ii), which aims to capture also the behavior around $\psi(2S)$.

(ii) A resonance $\psi(3770)$ and a bound state $\psi(2S)$: In addition to the Breit-Wigner form (5.4), which is linear in p^2, we make use also of the square form in p^2

$$\frac{p^3}{\sqrt{s}} \cot \delta_1(s) = A + Bp^2 + Cp^4 \tag{5.6}$$

which in general has a longer range of applicability. It aims to capture also the $\bar{D}D$ scattering in the vicinity of $\psi(2S)$: there the (imaginary) phase shift in Table 3 nearly satisfies the condition for the bound state $\cot \delta \simeq i$ on the physical Riemann sheet $p_B = i|p_B|$, leading to $p^3 \cot \delta \simeq |p_B|^3$. The fit (5.6) through levels $n = 2, 3, 5$ in Fig. 4 assumes that the $\psi(2S)$ state still affects the $\bar{D}D$ scattering. It renders $(A, B, C) \simeq (0.0046(19)\ \text{GeV}^2, -0.168(27), -0.52(13)/\text{GeV}^2), (0.0069(88)\ \text{GeV}^2, -0.023(80), -0.30(68)/\text{GeV}^2)$ on ensemble (1) and ensemble (2) respectively. The zero of $p^3 \cot \delta_1/\sqrt{s}$, and the derivative at this zero, lead to the parameters of $\psi(3770)$ resonance in Table 5. This model also leads to a bound state $\psi(2S)$ at $p_B = i|p_B|$ where the scattering amplitude T (5.2) has a pole and $\cot \delta(p_B) = i$. The bound state mass m_B in Table 5 is indeed close to experimentally measured $\psi(2S)$.

The results from both fit (i) and fit (ii) on ensemble (2) are compatible with the experimental data[3] within large statistical uncertainties (see Table 5). Note that the higher-lying $\psi(4040)$ resonance does not influence the results for this ensemble, since it lies significantly higher than the relevant energy levels.

Confronting the results for $\psi(3770)$ from fit (i) on ensemble (1) with experiment gives a smaller resonance momentum p_R than in experiment, which we attribute to the unphysical threshold on ensemble (1) at $m_\pi \simeq 266$ MeV and the finite lattice spacing. The resonance mass m_R calculated as in Eq. 3.4 compares favorably. The coupling constant from fit (i) is to small compared to experiment which which is likely related to to the closeness of the $\psi(4040)$ resonance neglected in the analysis. The assumption that the resonance $\psi(4040)$ does not affect the energy level related to $D(1)\bar{D}(-1)$ is probably not justified on ensemble (1), where energy level lies higher (and closer to $\psi(4040)$) than on ensemble (2). Roughly estimating the effect by comparing the one-resonance and two-resonance scenarios, estimating g and p_R for $\psi(3770)$ and $\psi(4040)$ from available experimental data [49], the coupling we observe is consistent with this interpretation [4]. Given the possibly large influence from the $\psi(4040)$ we can not conclude that fit (ii) is better than fit (i) on this ensemble.

The resulting 1^{--} spectrum is summarized and compared to experiment in Fig. 5.

[3] Since we work in the isospin-symmetric limit we measure the sum of the neutral and charged decay modes; therefore we compare to the experimental value $g^2_{exp} = g^2_{D^0\bar{D}^0} + g^2_{D^+D^-}$ obtained from $\Gamma[\psi(3770) \to D_0\bar{D}_0] = g^2_{D^0\bar{D}^0} p^3/(6\pi s)$ and $\Gamma[\psi(3770) \to D^+D^-] = g^2_{D^+D^-} p^3/(6\pi s)$ [15]. Notice also that averaging the results from recent experiment resonance mass determinations for the $\psi(3770)$ leads to a value of $m_R^{exp} = 3778.1(1.2)$, much larger than the fit by the PDG (which relies on an experiment neglecting interference with non-resonant background) and consistent with the most recent results in [16].

[4] The maximal effect of $\psi(4040)$ is estimated by assuming that $\psi(4040)$ width is saturated by $D\bar{D}$ (instead of $D\bar{D}$, $D\bar{D}^*$, $D^*\bar{D}^*$ and other modes).

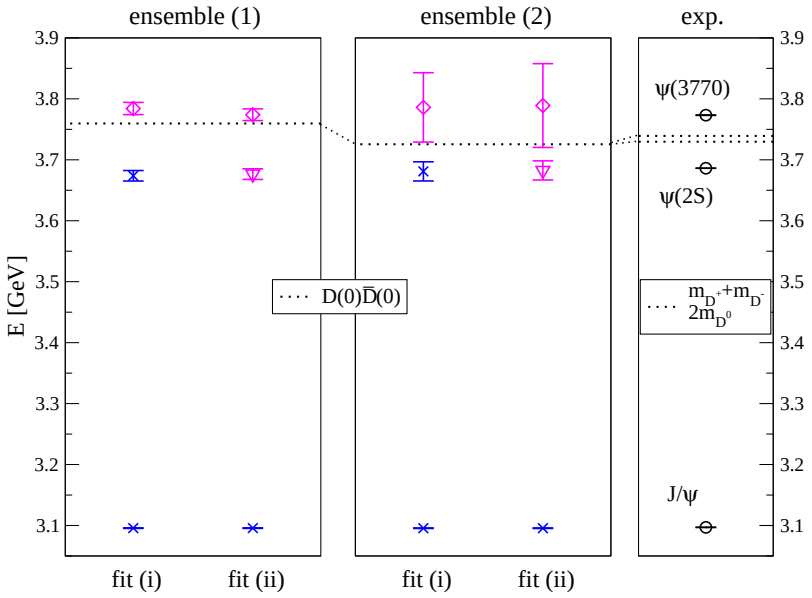

Figure 5. The comparison of the final 1^{--} spectrum to the experiment. The magenta diamond denotes $\psi(3770)$ resonance mass from the Breit-Wigner fit (i) or extended fit (ii), given in Eqs. (5.4) and (5.6), respectively. The magenta triangle denotes $\psi(2S)$ obtained as a pole in $D\bar{D}$ channel. The blue triangles denote masses of J/ψ and $\psi(2S)$ extracted as energy levels in the finite box. The statistical and scale setting errors have been summed in quadrature.

6 Results for the scalar channel

6.1 Discrete spectrum

The energy levels in the scalar channel are shown in Figs. 6. The only experimentally well established state is $\chi_{c0}(1P)$. The triangles represent the intriguing experimental candidates for $\chi_{c0}(2P)$, none of which is commonly accepted (see Section 2).

The spectrum from a lattice simulation consists both of energy levels that have large overlap with $\bar{q}q$ operators as well as energy levels with dominant overlap to $\bar{D}D$ operators. The latter appear near their non-interacting energies $E^{n.i.}_{DD}$ of Eq. (3.3), which are denoted by dashed lines in Figs. 6a,d. On ensemble (1) levels $n = 2, 4$ appear near the non-interacting $D(0)\bar{D}(0)$ and $D(1)\bar{D}(-1)$ (cf. Fig. 6a). Levels $n = 2, 3, 4$ on ensemble (2) have dominant overlap to $\bar{D}D$ scattering operators and are close to non-interacting $D(0)\bar{D}(0)$, $D(1)\bar{D}(-1)$ and $D(2)\bar{D}(-2)$ energies (cf. Fig. 6d).

Each energy level in addition to the number of expected $D(q)\bar{D}(-q)$ scattering levels is related to the presence of a bound state or a resonance. There are two such states, that cannot be attributed to $D(q)\bar{D}(-q)$ for both ensembles. The ground state is related to $\chi_{c0}(1P)$ and is close to its experimental mass. The second of these two levels appears above threshold and corresponds to $n = 3$ for ensemble (1) and $n = 5$ for ensemble (2), as shown in Figs. 6a and 6d. The avoided level crossing scenario suggests that an additional level appears somewhere in the range $E \simeq m \pm \Gamma$, which suggests the existence of a resonance

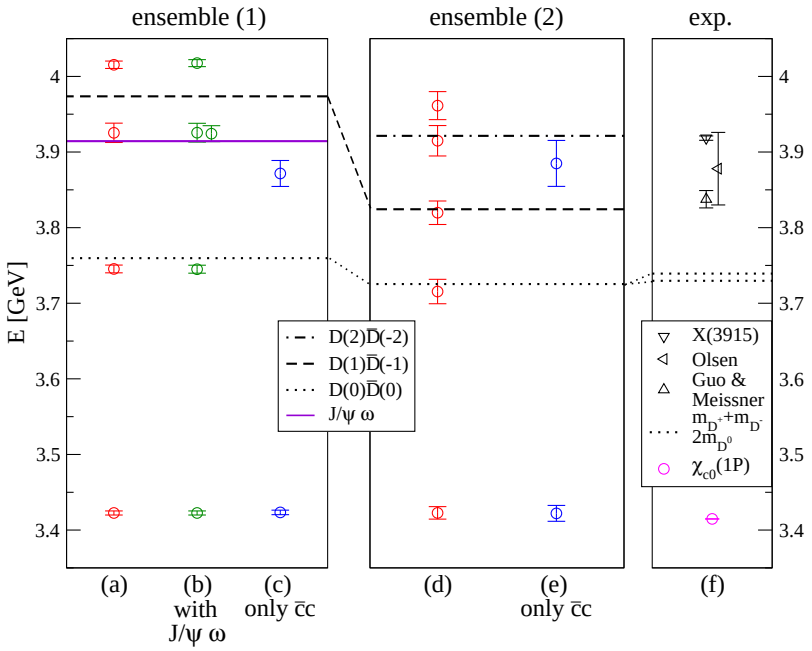

Figure 6. The energies E (see Eq. 3.4) in the scalar channel on both ensembles. The only well established experimental state $\chi_{c0}(1P)$ is shown by the (magenta) circle. Triangles show three intriguing candidates for $\chi_{c0}(2P)$, that are not universally accepted: $X(3915)$ and the broad resonances (2.1,2.2) suggested in [25, 26]. The dashed lines shown energies of non-interacting $D(q)\bar{D}(-q)$ with $q = 0, 1, 2$ (3.3), while dot-dashed line represents $m_{J/\psi} + m_\omega$. Interpolators used in (a,d) are given in Table 6, (b) uses $O^{J/\psi\,\omega}_{1,2}$ in addition, while (c,e) are based only on $O^{\bar{c}c}_{1,3,5}$.

roughly at

$$m \simeq 3.9 - 4.0 \text{ GeV} \quad \text{(naive estimate from } E_n\text{)} \,. \tag{6.1}$$

This is close to the first excitation obtained using just $O^{\bar{c}c}$ interpolators in Figs. 6c and 6e. Such a basis gives a rough estimate of resonance masses but is not well suited to capture two-particle states or resonances and bound states close to threshold [12–14].

The spectrum including $J/\psi\,\omega$ interpolating fields is shown in Fig. 6b for ensemble (1). An energy level related to $J/\psi(0)\,\omega(0)$ appears at roughly $m_{J/\psi} + m_\omega$ while the energies of all the other levels remain unaffected with respect to Fig. 6a. We have verified also that the overlaps for the remaining levels are not affected if $O^{J/\psi\,\omega}$ are in the basis or not. This indicates that the $J/\psi\,\omega$ channel is decoupled from $\bar{D}D$ channel to a good approximation.

6.2 $\bar{D}D$ scattering in s-wave

We now study $\bar{D}D$ scattering assuming that $J/\psi\,\omega$ channel is decoupled as argued in the previous paragraph. The energy shifts of the extracted E_n^{lat} with respect to $E_{DD}^{n.i.}$ give the size of the s-wave scattering phase shift δ according to (5.1). On ensemble (1) we observe statistically significant energy shifts with respect to the dashed lines in Fig. 6a. The energies yield D-meson momenta p via $E_n^{lat} = 2E_D(p)$, and the corresponding phase shifts

n	fit range	fit type	$\frac{\chi^2}{d.o.f.}$	$E^{lat}a$	E [GeV] (3.4)	$(ap)^2$	$(ap)\cot(\delta)$	$\frac{(ap)\cot(\delta)}{\sqrt{s}}$	$\delta[^\circ]$
	Ens.	(1)							
1	6-15	$2e^c$	9.50/6	1.7468(19)	3.4226(27)	−0.2226(49)	−0.4716(52)	−0.2700(31)	−240.9(2.8)i
2	6-15	$2e^c$	5.40/6	1.9494(33)	3.7453(52)	−0.0099(32)	0.11(11)	0.058(55)	4(190) + 84(306)i
3	3-12	$2e^c$	2.73/6	2.0625(81)	3.925(13)	0.1185(98)	0.39(17)	0.191(79)	41(11)
4	3-12	$2e^c$	6.39/6	2.1190(31)	4.0154(49)	0.1857(48)	−0.50(11)	−0.236(52)	139.2(6.5)
	Ens.	(2)							
1	4-15	$2e^c$	7.84/8	1.3672(38)	3.4227(83)	−0.1136(60)	−0.3371(89)	−0.2466(68)	−344.9(8.8)i
2	4-15	$2e^c$	3.74/8	1.5018(74)	3.715(16)	−0.0038(61)	−0.004(185)	−0.003(123)	−4(201)i
3	3-12	$2e^c$	3.50/6	1.5497(71)	3.820(16)	0.0367(61)	1.2(7.5)	0.8(4.8)	8.7(29.2)
4	6-12	$1e^c$	0.89/5	1.5934(92)	3.915(20)	0.0745(80)	1.7(10.8)	1.1(6.8)	9.1(28.3)
5	6-12	$1e^c$	1.68/5	1.6148(85)	3.961(19)	0.0932(75)	−0.21(21)	−0.13(13)	124(28)

Table 6. Discrete lattice spectrum for the scalar channel. The p and δ correspond to $\bar{D}D$ scattering in s-wave. Subset $O^{\bar{c}c}_{1,3,5}, O^{DD}_{1-3}$ from interpolators in Eq. (4.1) is used for ensemble (1) and $O^{\bar{c}c}_{1,3,5}, O^{DD}_{1,3,4}$ for ensemble (2). $t_0 = 2$ is used for all data points.

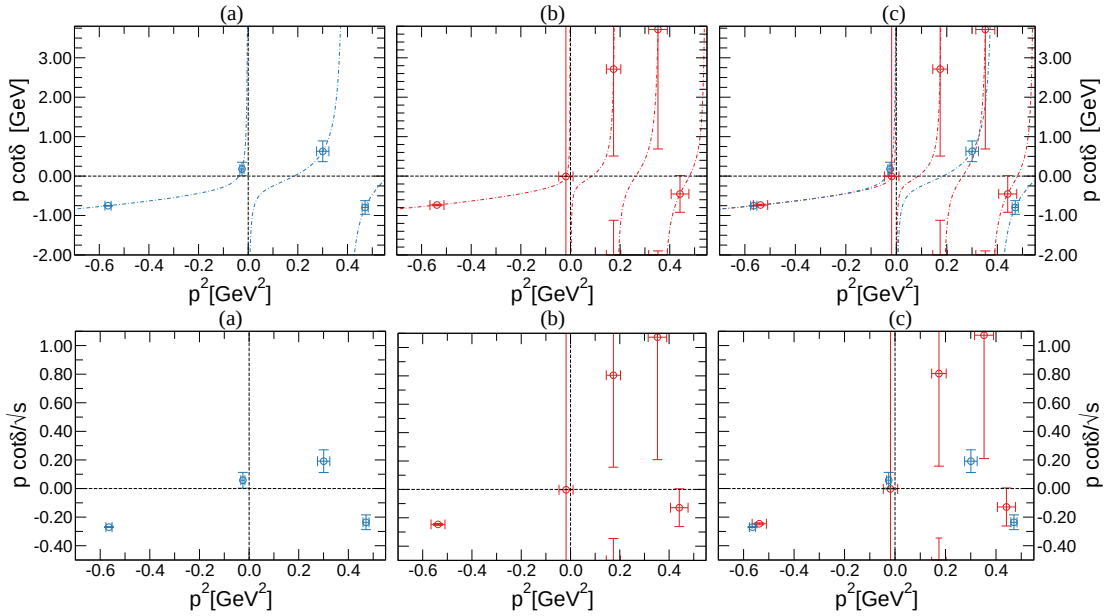

Figure 7. We show $p\cot\delta$ and $p\cot\delta/\sqrt{s}$ versus p^2 for $\bar{D}D$ scattering in s-wave, where p denotes the momentum of the D meson. The circles with (sizable) errors denote the lattice data, while the solid lines show $p\cot\delta = 2Z_{00}/(L\sqrt{\pi})$ according to Lüscher's relation (5.1). When the momentum is compatible with the non-interacting momentum $\mathbf{p} = 2\pi\mathbf{q}/L$ ($\mathbf{q} \in N^3$), one has $\delta = 0$ and $|\cot\delta| = \infty$, which is responsible for the huge errors on $p\cot\delta$ on ensemble (2).

$\delta(p)$ via Eq. (5.1). These are provided for all levels in Table 6 and plotted in Figs. 7 and 8.

The uncertainties on the energies $E_{n=2,3,4}$ are rather large for ensemble (2) and they are within errors compatible with non-interacting energies $E^{n.i.}_{DD}$ (3.3). This implies that we are

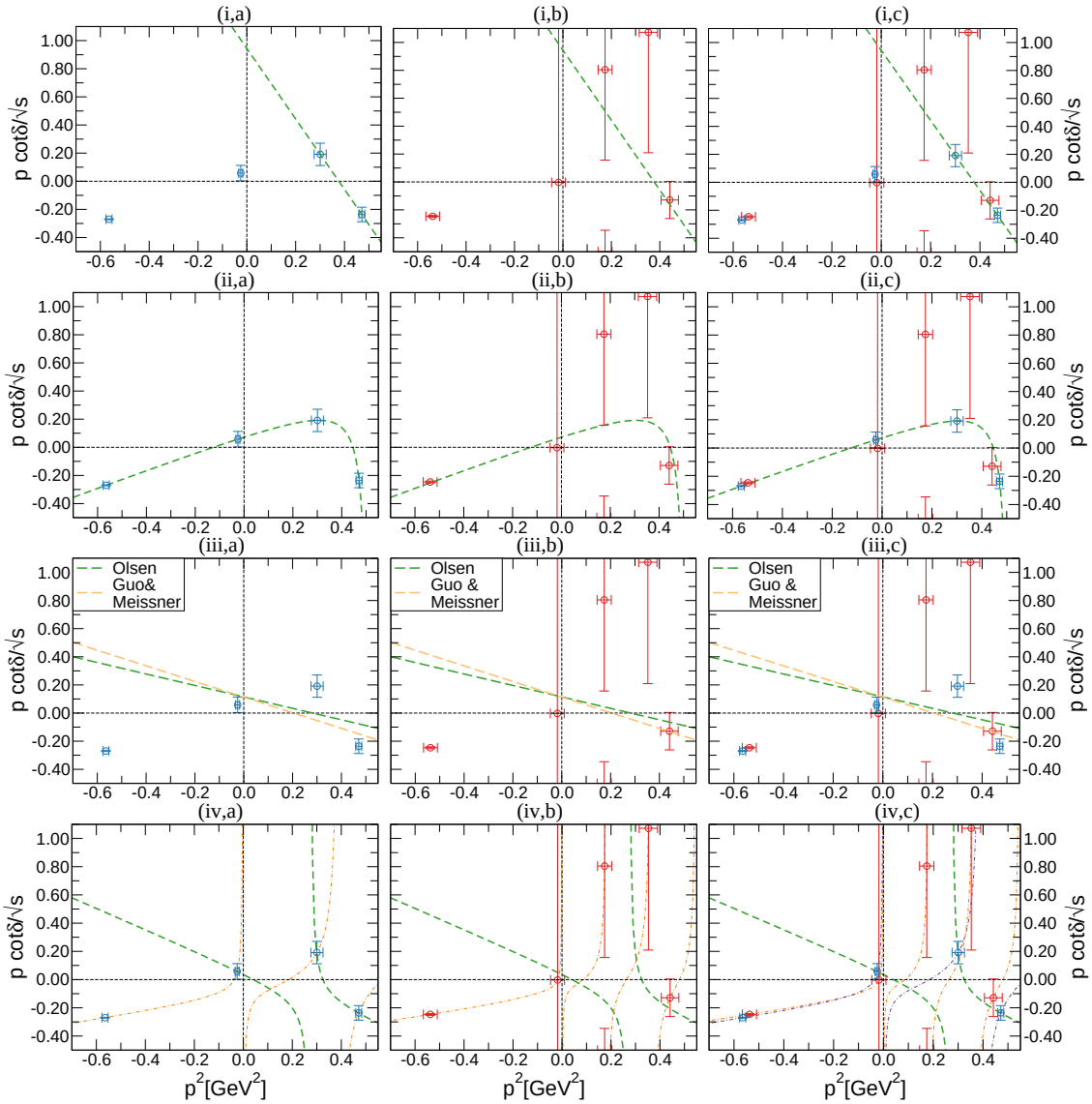

Figure 8. The $p\cot\delta/\sqrt{s}$ versus p^2 for $\bar{D}D$ scattering in s-wave, where p denotes the momentum of the D meson. The lattice data (blue and red circles) is confronted with $p\cot\delta/\sqrt{s}$ based on various hypothesis (dashed lines) described in Section 6 of the main text. The thin dot-dashed lines in the plots at the bottom denote $p\cot\delta = 2Z_{00}/(L\sqrt{\pi})$ (5.1).

not able to reliably determine the energy shifts, and the resulting errors on the scattering matrix will be large, as illustrated in Fig. 7. If $E_n^{lat} \simeq E_{DD}^{n.i.}$ within errors, this implies $\delta \simeq 0$ modulo π and $\cot\delta \simeq \pm\infty$ within errors. The extracted $p\cot\delta$ from $n = 2, 3, 4$ have large errors, which allow almost all $p\cot\delta$ expect for small $|p\cot\delta|$. For $n = 2, 3, 4$ we plot central values $f(p^2)$ with the ranges $[f(p^2 - \sigma_{p^2}), f(p^2 + \sigma_{p^2})]$ where $f = p\cot\delta$ or $p\cot\delta/\sqrt{s}$. The error for all other levels (on both ensembles and both channels) is the usual jack-knife.

The resulting $p\cot\delta/\sqrt{s}$ for ensemble (1) has a puzzling behavior and we are going to confront it with various hypothesis, collected in Fig. 8. The errors of $p\cot\delta/\sqrt{s}$ on ensemble (2) are large and do not allow reliable fits. We will still compare data from ensemble (2) with fits that are based on ensemble (1), and plot them as function of p^2 on the same figure. Note that the slightly different positions of thresholds $2m_D$ on the two ensembles do not play a crucial role in the scalar channel, since the anticipated resonances and bound states are not expected very close to the threshold (in contrast to $\psi(3770)$ in the vector channel).

(i) A narrow resonance: In the vicinity of a Breit-Wigner resonance (5.2) one expects

$$\frac{p\cot\delta(s)}{\sqrt{s}} = \frac{4}{g^2}(p_R^2 - p^2)\ , \quad \Gamma(s) = g^2\frac{p}{s} \tag{6.2}$$

and the zero gives the position of the resonance. The upper three points in Fig. 8a however do not fall onto one line, so our results cannot be reconciled with a single Breit-Wigner resonance in the region between $2m_D$ and 4 GeV. The highest two points support the existence of a narrow resonance between them and a linear fit (6.2) over two levels shown in Fig. 8(i,a) renders (5.5)

$$\begin{aligned} m_R &= 3.966(20)\ \text{GeV},\ g = 1.26(18)\ \text{GeV}, \\ p_R^{lat} &= 0.614(33)\ \text{GeV},\ \Gamma^{lat} = 62(17)\ \text{MeV}\ . \end{aligned} \tag{6.3}$$

The scattering data from ensemble (1) therefore suggest the existence of a yet unobserved scalar state called χ'_{c0}. Note that its mass is within the range of the naive estimate (6.1). It has a width Γ^{lat} in our simulation, while the corresponding width $g^2\tilde{p}/m_R^2$ in experiment would be modified due to a different phase space via $\tilde{p} = [m_R^2/4 - (m_D^{exp})^2]^{1/2}$, leading to

$$\Gamma^{exp}_{predict} = 67(18)\ \text{MeV}\ . \tag{6.4}$$

We have assumed that g and m_R do not depend on the pion mass here. It is unlikely that this state corresponds to $X(3915)$ since the $\bar{D}D$ decay channel was not observed for this state. A narrow resonance is roughly consistent also with the result from ensemble (2) within huge errors (see Fig. 8(i,b)), however there must be some additional interaction between D and $\bar{D}$ near the threshold according to ensemble (1).

(ii) A narrow resonance and a bound state $\chi_{c0}(1P)$: Our next hypothesis assumes that $\chi_{c0}(1P)$ represents a pole in $\bar{D}D$ scattering on the first Riemann sheet, leading to $p\cot\delta \simeq i|p_B|i = -|p_B|$ at the position of the bound state. The negative value of $p\cot\delta$ below threshold might be a possible reason why $p\cot\delta$ at threshold is smaller than expected based on narrow resonance (6.2,6.3). In this case the value of $p\cot\delta$ at threshold is influenced by the resonance and a bound state. To investigate this situation, we attempted several fits over all four levels on ensemble (1). A form that is motivated by our data

$$\frac{p\cot\delta(s)}{\sqrt{s}} = A + B\ p^2 + \frac{C}{p^2 - D} \tag{6.5}$$

is presented in Fig. 8(ii,a), where $A = 0.13(15)$, $B = 0.66(18)/\text{GeV}^2$, $C = 0.028(63)$ GeV^2 and $D = 0.513(77)$ GeV^2 are obtained from the fit. This hypothesis supports a bound state at $p_B = i|p_B|$ which corresponds to a pole in T (5.2) or equivalently $\cot\delta(p_B) = i$, i.e.

$$|p_B| = 0.7517(83) \text{ GeV} \quad m_B = 3.4224(27) \text{ GeV} . \tag{6.6}$$

The bound state is attributed to $\chi_{c0}(1P)$ and its mass is very close to the one obtained from the ground state energy. The hypothesis also supports a narrow resonance at $p_R = 0.668(35)$ GeV where function (6.5) crosses zero, and

$$\begin{aligned} m_R &= 4.002(24) \text{ GeV}, \; g = 0.85(65) \text{ GeV}, \\ \Gamma^{lat} &= 30(45) \text{ MeV} \; , \Gamma^{exp}_{predict} = 32(48) \text{ MeV} . \end{aligned} \tag{6.7}$$

This is roughly consistent with the χ'_{c0} in (6.3). This hypothesis based on ensemble (1) is consistent also with the result from ensemble (2) within huge errors in Fig. 8(ii,b). An interesting feature of this hypothesis is the large $p\cot\delta$ or equivalently small cross-section at $p^2 \simeq D$, which corresponds to $\sqrt{s} \simeq 4.0$ GeV. This feature seems to be present also in the experimental data from Belle [26] where a dip seems to appear at similar invariant mass.

(iii) A broad resonance: The broad resonances (2.1,2.2) proposed by Meissner&Guo [25] or Olsen [26] are confronted with our lattice data in Fig. 8(iii). This shows a Breit-Wigner shape (6.2) with p_R and g extracted from the experimental data (2.1,2.2). Although they are roughly compatible with our scattering results near threshold, they cannot be reconciled with it in the region above threshold where our data indicates either a much narrower resonance or a more complicated situation.

(iv) Two resonances: Since neither one narrow or one broad resonance describe our scattering data near and above threshold, we next try an hypothesis with two elastic resonances

$$\frac{p\cot\delta(s)}{\sqrt{s}} = \left[\frac{g_A^2}{4(p_{R_A}^2 - p^2)} + \frac{g_B^2}{4(p_{R_B}^2 - p^2)}\right]^{-1} . \tag{6.8}$$

With this parametrisation there are two resonance poles in the scattering amplitude, separated by a zero. Figure 8(iv,a) shows an example with $g_A = 2.1$ GeV, $p_{R_A} = 0.23$ GeV, $g_B = 1.0$ GeV and $p_{R_B} = 0.57$ GeV that is consistent with the upper three scattering points for ensemble (1)[5]. This hypothesis however predicts another energy level near $p^2 \simeq 0.1$ GeV^2 where the model (6.8) crosses with the Lüscher curve. Another energy level is expected in the two-resonance scenario also according to naive reasoning that each resonance or bound state leads to a level in addition to $\bar{D}D$. Such an additional energy level at $p^2 \simeq 0.1$ GeV^2 is not observed in ensemble (1) indicating that this hypothesis is not supported by our data. An analogous conclusion is reached when confronting this hypothesis with the data from ensemble (2): the hypothesis predicts five energy levels in the region $p^2 = [-0.1, 0.5]$ GeV and we observe four levels only.

[5] These values are not obtained from a fit, but present one example of four parameters, where (6.8) is consistent with upper three scattering points.

7 Conclusions and outlook

We performed a lattice QCD simulation of $\bar{D}D$ scattering in s-wave and p-wave to study vector and scalar charmonium resonances on two rather different ensembles. This is a first simulation aimed at determining the strong decay width of charmonium resonances above open charm threshold. Ensemble (1) has $N_f = 2$ and $m_\pi = 266$ MeV, while ensemble (2) has $N_f = 2 + 1$ and $m_\pi = 156$ MeV. Several $\bar{c}c$ and $D\bar{D}$ interpolating fields were used in both channels, where the (stochastic) distillation method was used to evaluate the Wick contractions.

In the vector channel, the well known $\psi(3770)$ resonance is present just above $\bar{D}D$ threshold. The phase shift for $D\bar{D}$ scattering in p-wave was determined using the Lüscher formalism. We performed a Breit-Wigner fit in vicinity of the $\psi(3770)$ to obtain its resonance mass at 3.784(7)(10) GeV and 3.786(56)(10) GeV for ensembles (1) and (2), respectively. Our determination of its decay width might be affected by the $\Psi(4040)$ on ensemble (1). Ensemble (2) does not suffer from this issue, and the determination of the resonance parameters is more reliable, but its statistical accuracy is poor. The resulting spectrum in the vector channel, including also J/ψ and $\psi(2S)$, is compared to experiment in Figure 5. This work presents a first step towards a determination of the $\psi(3770)$ resonance parameters from lattice QCD. Future lattice studies in multiple volumes (and or using multiple momentum frames) with a larger ensemble size should provide precision results for this resonance.

In the scalar channel, only the ground state $\chi_{c0}(1P)$ is understood and there is no commonly accepted candidate for its first excitation $\chi_{c0}(2P)$. Guo & Meissner [25] as well as Olsen [26] argued that the higher lying $X(3915)$ can probably not be identified with the $\chi_{c0}(2P)$. They suggest that a broad structure observed in $D\bar{D}$ invariant mass represents $\chi_{c0}(2P)$. This posed a particular motivation to extract the phase shift for $D\bar{D}$ scattering in s-wave in the present work. The resulting scattering data on the ensemble with $m_\pi = 156$ MeV is unfortunately noisy. The simulation at $m_\pi = 266$ MeV renders the scattering phase shift only at a few values of the $D\bar{D}$ invariant mass, which also does not allow a clear answer to the puzzles in this channel. We obtain the $\chi_{c0}(1P)$ and our data provides an indication for a yet-unobserved narrow resonance slightly below 4 GeV with $\Gamma[\chi'_{c0} \to D\bar{D}]$ below 100 MeV. A scenario with this narrow resonance and a pole in the $D\bar{D}$ scattering matrix at $\chi_{c0}(1P)$ agrees with the energy-dependence of our phase shift. We checked the consistency of other three scenarios with our data: just one narrow resonance, just one broad resonance proposed in Guo & Meissner [25] and Olsen [26], or one narrow and one broad resonance. None of these three scenarios agree with our data in the whole energy region we probed. For the scalar channel this leaves us with a situation where puzzles remain, both from theory and experiment. To clarify the situation, further experimental and lattice QCD efforts are required to map out the s-wave $D\bar{D}$ scattering in more detail.

Acknowledgments

We thank Anna Hasenfratz and the PACS-CS for providing the gauge configurations and Martin Lüscher for making his DD-HMC software available. The calculations were performed on computing clusters at TRIUMF, the University of Graz (NAWI Graz) and at Jozef Stefan Institute. This work is supported in part by the Austrian Science Fund FWF: I1313-N27, by the Slovenian Resarch Agency ARRS project N1-0020. Fermilab is operated by Fermi Research Alliance, LLC under Contract No. De-AC02-07CG11359 with the United States Department of Energy. S.P. acknowledges support from U.S. Department of Energy contract DE-AC05-06OR23177, under which Jefferson Science Associates, LLC, manages and operates Jefferson Laboratory.

References

[1] D. Mohler, C. DeTar, A. S. Kronfeld, S-H. Lee, L. Levkova, et al., *Low lying charmonium states at the physical point*, arXiv:1412.1057.

[2] B. Galloway, P. Knecht, J. Koponen, C. Davies, and G. Lepage, *Radial and orbital excitation energies of charmonium*, *PoS* **LATTICE2014** (2014) 092, [arXiv:1411.1318].

[3] D. Becirevic, M. Kruse, and F. Sanfilippo, *Lattice QCD estimate of the $\eta_c(2S) \to J/\psi\gamma$ decay rate*, arXiv:1411.6426.

[4] G. Donald, C. Davies, R. Dowdall, E. Follana, K. Hornbostel, et al., *Precision tests of the J/ψ from full lattice QCD: mass, leptonic width and radiative decay rate to η_c*, *Phys.Rev.* **D86** (2012) 094501, [arXiv:1208.2855].

[5] N. Brambilla, S. Eidelman, P. Foka, S. Gardner, A. Kronfeld, et al., *QCD and Strongly Coupled Gauge Theories: Challenges and Perspectives*, arXiv:1404.3723.

[6] A. Esposito, A. L. Guerrieri, F. Piccinini, A. Pilloni, and A. D. Polosa, *Four-Quark Hadrons: an Updated Review*, arXiv:1411.5997.

[7] G. S. Bali, S. Collins, and C. Ehmann, *Charmonium spectroscopy and mixing with light quark and open charm states from $n_F=2$ lattice QCD*, *Phys.Rev.* **D84** (2011) 094506, [arXiv:1110.2381].

[8] S. Ozaki and S. Sasaki, *Lúscher's finite size method with twisted boundary conditions: an application to J/ψ-ϕ system to search for narrow resonance*, *Phys.Rev.* **D87** (2013) 014506, [arXiv:1211.5512].

[9] S. Prelovsek and L. Leskovec, *Evidence for X(3872) from DD^* scattering on the lattice*, *Phys.Rev.Lett.* **111** (2013) 192001, [arXiv:1307.5172].

[10] **Fermilab Lattice Collaboration, MILC Collaboration** Collaboration, S-H. Lee, C. DeTar, H. Na, and D. Mohler, *Searching for the $X(3872)$ and $Z_c^+(3900)$ on HISQ lattices*, arXiv:1411.1389.

[11] **Hadron Spectrum Collaboration** Collaboration, L. Liu et al., *Excited and exotic charmonium spectroscopy from lattice QCD*, *JHEP* **1207** (2012) 126, [arXiv:1204.5425].

[12] C. B. Lang, D. Mohler, S. Prelovsek, and M. Vidmar, *Coupled channel analysis of the ρ meson decay in lattice QCD*, *Phys. Rev. D* **84** (2011) 054503, [arXiv:1105.5636].

[13] J. J. Dudek, R. G. Edwards, and C. E. Thomas, *Energy dependence of the ρ resonance in $\pi\pi$ elastic scattering from lattice QCD*, *Phys.Rev.* **D87** (2013) 034505, [arXiv:1212.0830].

[14] D. Mohler, S. Prelovsek, and R. M. Woloshyn, *$D\pi$ scattering and D meson resonances from lattice QCD*, *Phys.Rev.* **D87** (2013) 034501, [arXiv:1208.4059].

[15] **Particle Data Group** Collaboration, K. Olive et al., *Review of Particle Physics*, *Chin.Phys.* **C38** (2014) 090001.

[16] V. Anashin, V. Aulchenko, E. Baldin, A. Barladyan, A. Y. Barnyakov, et al., *Measurement of $\psi(3770)$ parameters*, *Phys.Lett.* **B711** (2012) 292–300, [arXiv:1109.4205].

[17] J. L. Rosner, *Charmless final states and S-D wave mixing in the Ψ''*, *Phys.Rev.* **D64** (2001) 094002, [hep-ph/0105327].

[18] J. L. Rosner, *Ψ'' decays to charmless final states*, *Annals Phys.* **319** (2005) 1–12, [hep-ph/0411003].

[19] E. Eichten, S. Godfrey, H. Mahlke, and J. L. Rosner, *Quarkonia and their transitions*, *Rev.Mod.Phys.* **80** (2008) 1161–1193, [hep-ph/0701208].

[20] **BES Collaboration** Collaboration, M. Ablikim et al., *Direct measurements of the cross sections for $e^+e^- \to$ hadrons (non-$D\bar{D}$) in the range from 3.65-GeV to 3.87-GeV and the branching fraction for $\psi(3770) \to$ non-$D\bar{D}$*, *Phys.Lett.* **B659** (2008) 74–79.

[21] **CLEO Collaboration** Collaboration, D. Besson et al., *Measurement of $\sigma(e^+e^- \to \psi(3770) \to$ hadrons) at $E_{c.m.} = 3773$ MeV*, *Phys.Rev.Lett.* **96** (2006) 092002, [arXiv:1004.1358].

[22] P. Wang, C. Yuan, and X. Mo, *Possible large branching fraction of psi-prime-prime decays to charmless final states*, *Phys.Rev.* **D70** (2004) 114014, [hep-ph/0410300].

[23] C. DeTar, A. Kronfeld, S-H. Lee, L. Levkova, D. Mohler, et al., *Charmonium mass splittings at the physical point*, *PoS* **LATTICE2012** (2012) 257, [arXiv:1211.2253].

[24] **BaBar Collaboration** Collaboration, J. Lees et al., *Study of $X(3915) \to J/\psi\omega$ in two-photon collisions*, *Phys.Rev.* **D86** (2012) 072002, [arXiv:1207.2651].

[25] F.-K. Guo and U.-G. Meissner, *Where is the $\chi_{c0}(2P)$?*, *Phys.Rev.* **D86** (2012) 091501, [arXiv:1208.1134].

[26] S. L. Olsen, *Is the X(3915) the $\chi_{c0}(2P)$?*, arXiv:1410.6534.

[27] **BaBar Collaboration** Collaboration, B. Aubert et al., *Observation of the $\chi_{c2}(2P)$ meson in the reaction $\gamma\gamma \to D\bar{D}$ at BABAR*, *Phys.Rev.* **D81** (2010) 092003, [arXiv:1002.0281].

[28] **Belle Collaboration** Collaboration, S. Uehara et al., *Observation of a χ'_{c2} candidate in $\gamma\gamma \to D\bar{D}$ production at BELLE*, *Phys.Rev.Lett.* **96** (2006) 082003, [hep-ex/0512035].

[29] **Belle Collaboration** Collaboration, P. Pakhlov et al., *Production of New Charmoniumlike States in $e^+e^- \to J/\psi D^{(*)}\bar{D}^{(*)}$ at $\sqrt{s} \sim 10$ GeV*, *Phys.Rev.Lett.* **100** (2008) 202001, [arXiv:0708.3812].

[30] S. Prelovsek, L. Leskovec, and D. Mohler, *Charmonium-like states from scattering on the lattice*, *PoS* **LATTICE2013** (2013) 254, [arXiv:1310.8127].

[31] A. Hasenfratz, R. Hoffmann, and S. Schaefer, *Reweighting towards the chiral limit*, *Phys. Rev. D* **78** (2008) 014515, [arXiv:0805.2369].

[32] A. Hasenfratz, R. Hoffmann, and S. Schaefer, *Low energy chiral constants from epsilon-regime simulations with improved Wilson fermions*, *Phys. Rev. D* **78** (2008) 054511, [arXiv:0806.4586].

[33] **PACS-CS Collaboration** Collaboration, S. Aoki et al., *2+1 Flavor Lattice QCD toward the Physical Point*, *Phys.Rev.* **D79** (2009) 034503, [arXiv:0807.1661].

[34] C. B. Lang, L. Leskovec, D. Mohler, S. Prelovsek, and R. M. Woloshyn, *D_s mesons with DK and D^*K scattering near threshold*, *Phys.Rev.* **D90** (2014) 034510, [arXiv:1403.8103].

[35] A. X. El-Khadra, A. S. Kronfeld, and P. B. Mackenzie, *Massive Fermions in Lattice Gauge Theory*, *Phys. Rev.* **D55** (1997) 3933–3957, [hep-lat/9604004].

[36] M. B. Oktay and A. S. Kronfeld, *New lattice action for heavy quarks*, *Phys. Rev. D* **78** (2008) 014504, [arXiv:0803.0523].

[37] **Fermilab Lattice Collaboration, MILC Collaboration** Collaboration, C. Bernard et al., *Tuning Fermilab Heavy Quarks in 2+1 Flavor Lattice QCD with Application to Hyperfine Splittings*, *Phys.Rev.* **D83** (2011) 034503, [arXiv:1003.1937].

[38] A. S. Kronfeld, *Application of heavy quark effective theory to lattice QCD. 1. Power corrections*, *Phys.Rev.* **D62** (2000) 014505, [hep-lat/0002008].

[39] D. Mohler, C. B. Lang, L. Leskovec, S. Prelovsek, and R. M. Woloshyn, *$D^*_{s0}(2317)$ Meson and D-Meson-Kaon Scattering from Lattice QCD*, *Phys.Rev.Lett.* **111** (2013), no. 22 222001, [arXiv:1308.3175].

[40] **Hadron Spectrum Collaboration** Collaboration, M. Peardon, J. Bulava, J. Foley, C. Morningstar, J. Dudek, R. G. Edwards, B. Joo, H.-W. Lin, D. G. Richards, and K. J. Juge, *A novel quark-field creation operator construction for hadronic physics in lattice QCD*, *Phys. Rev. D* **80** (2009) 054506, [arXiv:0905.2160].

[41] C. Morningstar, J. Bulava, J. Foley, K. J. Juge, D. Lenkner, M. Peardon, and C. H. Wong, *Improved stochastic estimation of quark propagation with Laplacian Heaviside smearing in lattice QCD*, *Phys. Rev. D* **83** (2011) 114505, [arXiv:1104.3870].

[42] J. J. Dudek, R. G. Edwards, N. Mathur, and D. G. Richards, *Charmonium excited state spectrum in lattice QCD*, *Phys. Rev. D* **77** (2008) 034501, [arXiv:0707.4162].

[43] C. Michael, *Adjoint Sources in Lattice Gauge Theory*, *Nucl. Phys. B* **259** (1985) 58.

[44] M. Lüscher, *Volume dependence of the energy spectrum in massive quantum field theories. I. Stable particle states*, *Commun. Math. Phys.* **104** (1986) 177.

[45] M. Lüscher and U. Wolff, *How to calculate the Elastic Scattering Matrix in 2-Dimensional QuantumField Theories by Numerical Simulation*, *Nucl. Phys. B* **339** (1990) 222.

[46] B. Blossier, M. DellaMorte, G. von Hippel, T. Mendes, and R. Sommer, *On the generalized eigenvalue method for energies and matrix elements in lattice field theory*, *JHEP* **0904** (2009) 094, [arXiv:0902.1265].

[47] M. Lüscher, *Two-Particle States on a Torus and Their Relation to the ScatteringMatrix*, *Nucl. Phys. B* **354** (1991) 531.

[48] M. Lüscher, *Signatures of unstable particles in finite volume*, *Nucl. Phys. B* **364** (1991) 237.

[49] **BaBar Collaboration** Collaboration, B. Aubert et al., *Exclusive Initial-State-Radiation Production of the $D\bar{D}$, $D\bar{D}^*$, and $D^*\bar{D}^*$ Systems*, *Phys.Rev.* **D79** (2009) 092001, [arXiv:0903.1597].